



Nearly degenerate ground state of phosphorus donor in diamond

C. Shinei ¹, H. Kato,² H. Watanabe,² T. Makino,² S. Yamasaki,² S. Koizumi,³ and T. Umeda ^{1,*}

¹*Institute of Applied Physics, University of Tsukuba, Tsukuba, 305-0006, Japan*

²*National Institute of Advanced Industrial Science and Technology (AIST), Tsukuba, 305-8568, Japan*

³*National Institute for Materials Science (NIMS), Tsukuba, 305-0044, Japan*



(Received 18 November 2019; revised manuscript received 27 January 2020; accepted 11 February 2020; published 27 February 2020)

We investigate phosphorus (P) donors in P-doped diamond epitaxial films by means of electron paramagnetic resonance spectroscopy (EPR). In a diamond thin film on Ila diamond substrate, we could observe an EPR signal of the NIMS1 center, which has been assigned to a neutral P donor with a D_{2d} symmetry. In contrast, we could not observe this center in another free-standing diamond film with the same P concentration ($[P] \sim 1 \times 10^{17} \text{ cm}^{-3}$). This striking contrast can be reasonably accounted for in a model where the P donor in diamond has a nearly degenerate ground state due to t_2 and e , in contrast to P donors in group-IV semiconductors like Si and Ge, where a_1 singlet ground state is present. We observed a strong uniaxial strain only in the former diamond thin film, which was confirmed by Raman microscopy and preferential orientations of NIMS1 EPR centers. This strain splits the nearly degenerate ground state of the P donor, resulting in the observation of the NIMS1 center. We point out that the electronic system of the substitutional P donor in diamond is similar to that of interstitial Li donor in Si.

DOI: [10.1103/PhysRevMaterials.4.024603](https://doi.org/10.1103/PhysRevMaterials.4.024603)

I. INTRODUCTION

Diamond is a promising material for electronic devices of high frequency, high power, and high temperature applications [1], and is a host material for quantum technologies using a nitrogen-vacancy (NV) center with a long coherence time [2]. From the viewpoints of both power electronics and quantum applications, a critical issue is how to control the Fermi levels of this material by n - and p -type doping diamond with phosphorus (P) and boron (B) impurities, respectively. The P doping of diamond is much more difficult than the B doping [3]. Therefore, there is less understanding of the n -type diamond and its doping mechanism [4]. In addition, an unexpected phenomenon was recently reported that the P doping can enhance the coherence time of the NV centers [5]. Generally, their coherence time is significantly reduced by the surrounding electron and nuclear spins of the impurities in diamond. However, practical behavior of the P donors is opposite to that of other impurities and still unclear. Therefore, it is important to understand the nature of the electron spins of P donors as well as the electronic structures of P donors in diamond.

The P donors in group-IV semiconductors such as Si [6], Ge [7], and SiC [8] can be easily observed by electron paramagnetic resonance (EPR). In n -type diamond films, EPR signals of P-related centers were reported by Samsonenko *et al.*, Zvanut *et al.*, Isoya *et al.*, Casanova *et al.*, Graf *et al.* [9–13], and Katagiri *et al.* [14]. Among these P-related centers, a spin-1/2 EPR center, called the National Institute for Material Science (NIMS)1 center [14], was assigned to

a neutral P donor, similar to the P donor signals in Si, Ge, and SiC (3C-, 4H-, and 6H-SiC). The NIMS1 center showed a D_{2d} symmetry, which originates from the t_{2z} ground state of the substitutional P donor with a D_{2d} -symmetric distortion [14]. Some theoretical calculations [15–17] supported these EPR observations, while others, including the effective-mass theory [18–23], predicted that the P donor in diamond should have a singlet a_1 ground state that is commonly found in P donors in other group-IV semiconductors. Therefore, the understanding of P donors in diamond is still controversial.

In this study, we propose a solution to this controversy by comparing two different types of P-doped diamond films. The two diamond films involved different lattice strains; only one P-doped film exhibited a strong uniaxial strain due to an undoped substrate. As a result, a strain-induced appearance of the P donor signal (the NIMS1 center) was observed. This phenomenon was quite similar to the case of Li donors in Si under uniaxial strain that have a nearly degenerate ground state of $t_2 + e$. We propose that P donors in diamond should have a similar nearly degenerate ground state of $t_2 + e$.

II. EXPERIMENTAL

As shown in Table I, two P-doped diamond films were epitaxially grown on a (111) surface of either a type-Ib HPHT substrate ($2 \times 2 \text{ mm}^2$) or type-Ila HPHT substrate ($2 \times 2 \text{ mm}^2$) by plasma-enhanced chemical vapor deposition. We call these two films “sample A” and “sample B”, respectively. The P doping of the two diamond films was carried out by mixing PH_3 (6N) with CH_4 (6N) and H_2 (9N) with the gas ratios shown in Table I. The two P-doped films with the same P concentration ($[P] \sim 1 \times 10^{17} \text{ cm}^{-3}$) were finally obtained with thicknesses of 45 and 10 μm for samples

*Corresponding author: umeda@bk.tsukuba.ac.jp

TABLE I. Epitaxial growth conditions of two P-doped diamond films.

	Sample A	Sample B
Microwave power	3600 W	450 W
Pressure	150 Torr	100 Torr
Temperature	900 °C	900 °C
CH ₄ /H ₂	0.4%	0.05%
PH ₃ /CH ₄	500 ppm	200 ppm
P doping	$\sim 1 \times 10^{17} \text{ cm}^{-3}$	$\sim 1 \times 10^{17} \text{ cm}^{-3}$

A and sample B, respectively. Their P concentrations were confirmed by secondary ion mass spectrometry (SIMS). To prepare a free-standing film, the base substrate of sample A was removed by laser cutting. The cut surface was polished, and the damaged layer was completely removed. Before the EPR measurements, the two P-doped films were chemically cleaned. To prepare a free-standing film, the base substrate of sample A was removed by laser cutting. The cut surface was polished, and the damaged layer was completely removed. Before the EPR measurements, the two P-doped films were chemically cleaned to remove surface contaminations using an acid mixture (H₂SO₄:HNO₃ = 3 : 1) at 230 °C for 30 min for sample A or a solution of NaClO₃ in HNO₃ at 200 °C for 3 h for sample B. Both the acid treatments cause O-termination of the sample surfaces. This termination simultaneously leads to removing hydrogen, graphite, amorphous carbon, and other contaminants on the surface. Thus, the two cleaning procedures gave the same effect to the two samples.

The EPR measurements were performed by a Bruker E500 continuous-wave X-band EPR spectrometer with a super-high-Q cavity and an Oxford ESR-900 continuous-flow He cryostat. The EPR spectra were measured at temperatures from 4 to 80 K. We used microwave excitation at 9.428 GHz and magnetic-field modulation at 100 kHz. The modulation amplitude was set to 0.02 mT. The magnetic field (\mathbf{B}) was rotated in the ($\bar{1}10$) plane. A magnetic-field angle of 0° corresponds to $\mathbf{B} // [111]$.

To confirm the P doping and the activation of the P donors, SIMS was carried out on the two P-doped films. Cathode luminescence (CL) of excitons bound on the P donors was observed at 80 K using a scanning electron microscope equipped with a liquid nitrogen cooling stage, an ellipsoidal mirror, and a monochromator fitted with a 300 grooves/mm grating. The CL signal was focused by the ellipsoidal mirror onto the entrance slit of the monochromator and detected with a charge-coupled device (CCD) camera. In the CL measurements, the accelerating voltage and the probe current were 13 kV and 100 nA, respectively.

To characterize the lattice strain in P-doped films, Raman microscopy was performed by a confocal microscope with a double-grating monochromator (Jobin-Yvon/Horiba U-1000) and a liquid-nitrogen-cooled CCD detector. The confocal spot was about 1 μm . The light source was a 532-nm green laser diode. The grating was 1800 grooves/mm. Three emission lines from a Ne lamp were used for the wavelength calibration. A diamond Γ -phonon Raman peak ($\sim 1330 \text{ cm}^{-1}$) was measured with a resolution of $< 0.02 \text{ cm}^{-1}$. We measured line

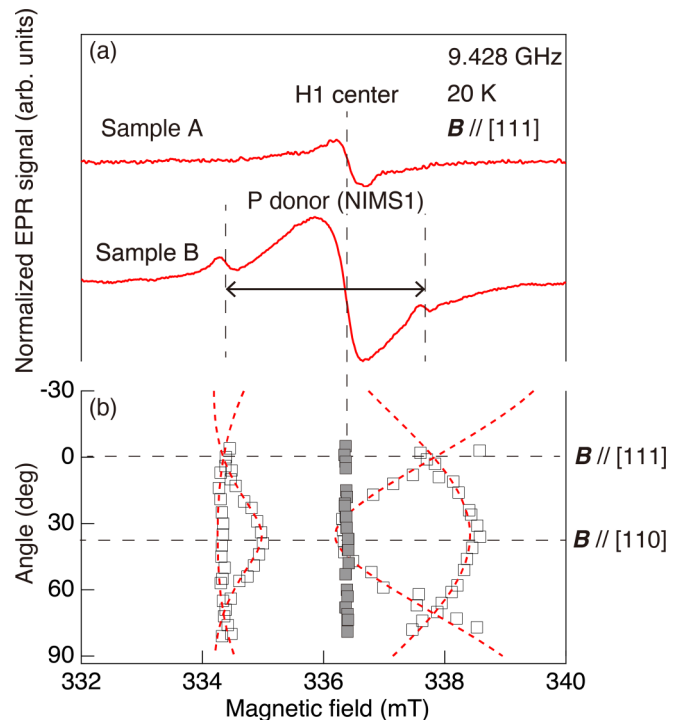


FIG. 1. (a) EPR spectra of P-doped diamond(111) epitaxial films. Only in sample B, was the NIMS1 center of shallow P donor observed, in addition to H1 center (a typical carbon defect in epitaxially grown diamond). (b) Angular dependence of EPR signals in sample B measured at 20 K. Open squares and solid squares correspond to NIMS1 center and H1 center, respectively. Dotted curves are simulated by EPR parameters of NIMS1 shown in Table II.

profiles on each edge face of the two P-doped samples by a step of 1 μm over a 150- μm length.

III. RESULTS

A. EPR observation of the NIMS1 center (neutral P donor)

In Fig. 1(a), the EPR spectra of the two P-doped films measured at 20 K are shown for $\mathbf{B} // [111]$. In both sample A and sample B, a common single peak is observed at the center of each spectrum. This EPR signal originates from the H1 center, which is a typical carbon defect in epitaxially grown diamonds [24]. Only in sample B, is a 3.4-mT doublet structure observed. This structure is identical to a ³¹P hyperfine (HF) structure of the NIMS1 center [14]. In Fig. 1(b), angular dependences of the observed EPR lines in sample B are shown, in addition to the known angular dependences of the NIMS1 center simulated by the EPR parameters shown in Table II. The simulated curves are in excellent agreement with

TABLE II. EPR parameters of NIMS1 center. $A_{\text{iso}} = (A_{\parallel} + 2A_{\perp})/3$ and $b = (A_{\parallel} - A_{\perp})/3$ [37]. In this work, we experimentally obtained $A_{\parallel} = 5.77 \text{ mT}$ and $A_{\perp} = 1.21 \text{ mT}$ for a [001]-axially symmetric ³¹P HF interaction.

	Symmetry	g_{\parallel}	g_{\perp}	A_{iso} (mT)	b (mT)
Ref. [14]	D_{2d}	1.9983	2.0072	2.73	1.52
Present: sample B	D_{2d}	1.9983	2.0072	2.73	1.52

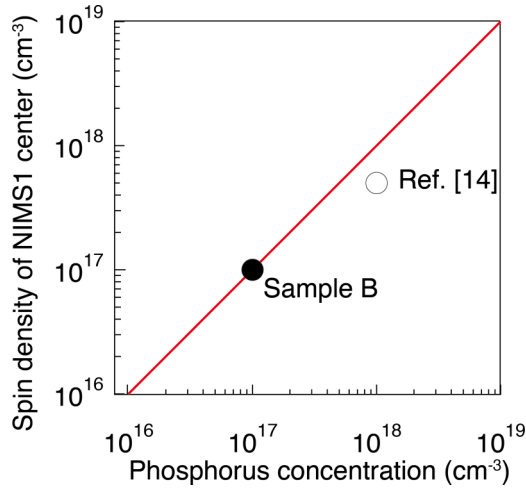


FIG. 2. Spin densities of NIMS1 center and P concentrations measured by SIMS. Open circle is referred from Ref. [14]. A solid line expresses one-to-one correlation between NIMS center and P doping.

the experimental data. These curves were calculated using the EPR parameters ($g_{//}$, g_{\perp} , $A_{//}$, and A_{\perp}) shown in Table II and the following spin Hamiltonian:

$$\mathcal{H} = \mu_B \mathbf{S} \cdot \mathbf{g} \cdot \mathbf{B} + \mathbf{S} \cdot \mathbf{A} \cdot \mathbf{I},$$

where μ_B is the Bohr magneton, \mathbf{S} is an electron spin operator ($S = 1/2$), \mathbf{g} is an axially symmetric gyromagnetic-factor (g -factor) tensor with principal values of $g_{//}$ and g_{\perp} , \mathbf{A} is an axially symmetric HF tensor with principal values of $A_{//}$ and A_{\perp} , and \mathbf{I} is a nuclear spin operator for a ^{31}P nucleus ($I = 1/2$). Figure 2 shows an approximate one-to-one correlation between the spin densities of the NIMS1 center and the P concentrations measured by SIMS. We conclude that the incorporated P atoms in sample B are activated as P donors in diamond. This result is consistent with a previous electrical characterization that the carrier concentration derived from

the Hall measurements is consistent with the P concentration measured by SIMS [25].

On the other hand, sample A only exhibits the H1 center as is shown in Fig. 3(a). Even at 4.2 K, we cannot observe the NIMS1 center with the donor concentration of $1 \times 10^{17} \text{ cm}^{-3}$ [dotted lines in Fig. 3(b)]. To confirm the activation of the P donor in sample A, we carried out the CL measurements (Fig. 4). The “FE_{TO}” and “BE_{TO}” CL signals, which originate from the free-exciton and bound-exciton luminescence, respectively, are detectable in sample A as well as in sample B. Thus, it is confirmed that the magnitude of the donor activation in sample A is as high as that in sample B.

The disappearing EPR signal of the NIMS1 center in sample A is attributed to a lifetime broadening phenomenon. In general, when an unpaired electron occupies a degenerate or nearly degenerate energy level, its EPR signal should disappear due to the lifetime broadening. However, the hidden EPR signal appears when a strong strain is applied and cancels the degeneracy. For instance, Watkins *et al.* [26] reported that the EPR signal of the Li donor in Si, which has a nearly degenerate ground state of $t_2 + e$, appeared when a uniaxial strain was applied to Li-doped Si crystals. Another example is seen in B-doped Si crystals: Feher *et al.* [27] revealed that the B acceptor has a degenerate ground state; hence, its EPR signal appeared only under a strong uniaxial strain. Therefore, it is reasonable to consider that the P donor in diamond has a (nearly) degenerate ground state similar to the above examples, and that a strong strain is present only in sample B, resulting in the appearance of the donor EPR signal (NIMS1 center). In the following two sections, we experimentally evaluate lattice strains in P-doped diamond films.

B. Lattice strain in P-doped diamond films studied by Raman shifts

A lattice strain is often evaluated by Raman shifts. Figure 5(a) shows cross-sectional line profiles of diamond

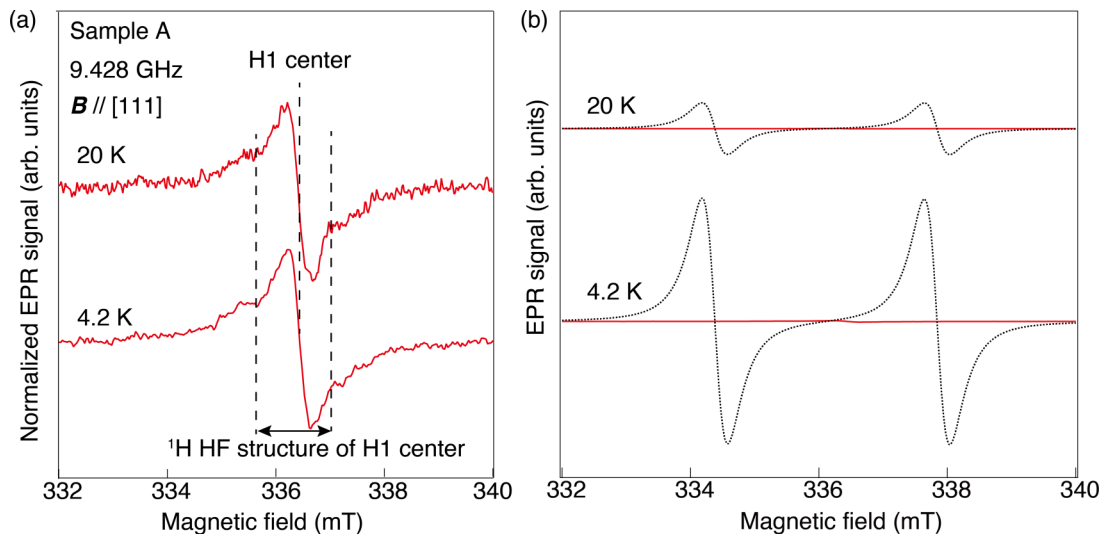


FIG. 3. EPR spectra of sample A measured at 20 and 4.2 K. (a) Only H1 center can be observed at both temperatures, where a 1.4-mT doublet structure indicates characteristic ^1H hyperfine interaction of H1 center. (b) Simulation of the NIMS1 EPR signal with spin density of $1 \times 10^{17} \text{ cm}^{-3}$ (dotted lines). The NIMS1 center was not detectable at either temperature. Vertical scale is common to both the 20 and 4.2 K signals.

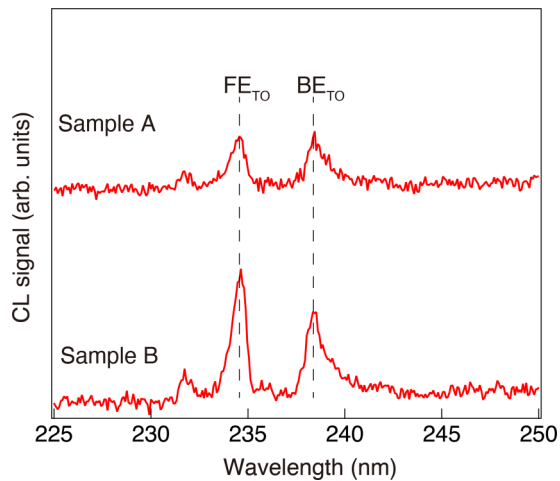


FIG. 4. CL spectra of sample A and sample B. “ FE_{TO} ” and “ BE_{TO} ” peaks originate from free excitons of diamond and binding excitons of neutral P donors, respectively. Vertical scale is common both to sample A and sample B.

Γ -phonon Raman peak on each edge face of samples A and B. To determine peak positions of the diamond Raman peak accurately at each focused point, we performed a fitting analysis

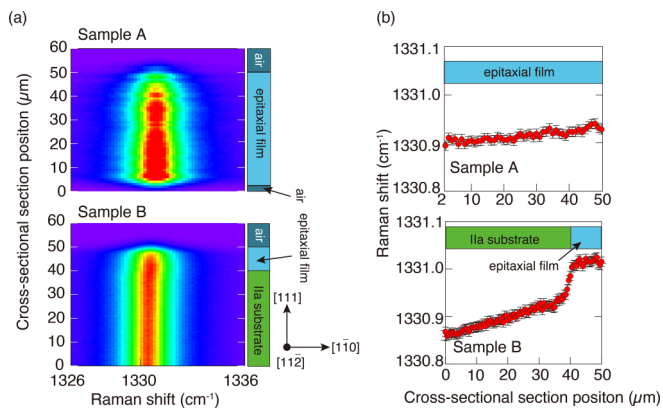


FIG. 5. (a) Cross-sectional Raman mapping of diamond Γ -phonon Raman peak on each edge face of sample A and sample B. In sample A, a free-standing P-doped epitaxial film is shown in the range between 2 and 50 μm . In sample B, regions over 50 μm indicate the air region. Raman spectra were measured at every 1- μm step on each edge face of samples. (b) Raman shifts as a function of cross-sectional positions. Only in sample B, was an irregular Raman shift of $+0.1 \text{ cm}^{-1}$ detected in the P-doped region, which is due to the presence of a strong compressive strain in this region (see details in text). In addition to the stepwise change, a gradual change in the Raman shift was also observed in sample B. Its magnitude depended on measured positions in sample B. Furthermore, base levels for the Raman shift varied from 1330.35 to 1331.25 cm^{-1} in sample B. Such behaviors may relate to an inhomogeneity of the IIa substrate of sample B. Regardless of the variations, the stepwise change of $+0.1 \text{ cm}^{-1}$ was always observed in every line profile of sample B. In sample A, a relatively weak gradual change was observed. Fluctuated Raman intensities in sample A may originate from a surface roughness of its edge face.

using a single Lorentzian peak. In Fig. 5(b), we plot the determined Raman shifts as a function of cross-sectional positions in samples A and B. In sample B only, a stepwise increase in the Raman shift was observed just at the boundary (40 μm) between the substrate and the P-doped film, suggesting the presence of a strong compressive strain in the P-doped film of sample B. The stepwise increase is about $+0.1 \text{ cm}^{-1}$, which approximately corresponds to a compressive strain of 40 or 150 MPa, supposing that either a hydrostatic strain [28] or a biaxial strain in the (111) plane [29] is applied to a diamond crystal. The above compressive strains are comparable to the uniaxial strains (6–90 MPa) applied to Li-doped and B-doped Si that could induce visible EPR signals of Li donors and B acceptors, respectively [26,27]. Therefore, we can reasonably expect that in sample B, the P donor shows a strain-induced EPR signal (the NIMS1 center).

The observed compressive strain is most probably due to the P doping of diamond. Since the atomic radius of P is 1.4 times larger than that of C, a P-doped diamond must expand compared to an undoped diamond. Therefore, in sample B, the P-doped epitaxial layer on the base substrate suffers from a strong compressive strain. In the next section, we further determine the direction of the compressive strain in sample B by examining the directions of the D_{2d} -symmetric distortions of the NIMS1 centers.

C. Lattice strain in P-doped diamond films studied by preferential orientations of NIMS1 EPR centers

Figure 6(a) shows a D_{2d} -symmetric distortion of the NIMS1 center or a substitutional P atom. A tetragonal D_{2d} symmetry generates three equivalent distorted orientations along the [100], [010], and [001] axes. In Fig. 6(b), an EPR spectrum of sample B for $B // [110]$ is shown, where two orientations of the NIMS1 centers ([001] and [100] + [010]) are distinguishable. We performed a spectrum simulation of the NIMS1 EPR signal for an ideal case (the NIMS1 centers uniformly exhibit the three equivalent orientations) and for a preferentially orientated case (the NIMS1 centers exhibit preferential orientations due to a uniaxial strain). As shown in Fig. 6(b), the preferential orientations are more probable. Figure 6(c) summarizes each population of the three orientations for the NIMS1 center. The preferential orientation along the [001] axis was confirmed in sample B. In principle, a NIMS1 center with a [001] orientation (shrinking along the [001] axis) is energetically favorable. This suggests the presence of a strong uniaxial strain along the [001] axis in the P-doped layer of sample B. This strong uniaxial strain causes the splitting of the nearly degenerate ground state of the NIMS1 center, as discussed in the next section. We confirmed using an x-ray diffraction measurement that the IIa substrate of sample B has an off-angle direction towards the $[\bar{1}\bar{1}2]$ axis, as shown in Fig. 6(d). This direction includes a more [001] component than [100] and [010] components. This may be related to the preferential orientation of the [001]-distorted NIMS1 center. We roughly speculate that P-induced strain may correlate with the off-angle direction, which may strengthen the strain along this direction.

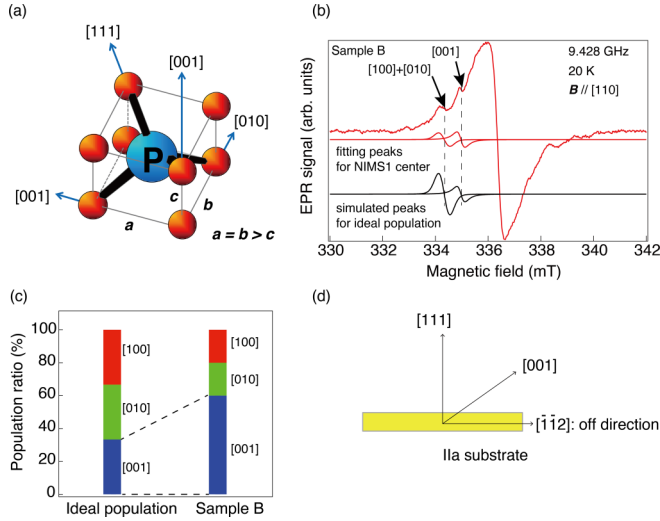


FIG. 6. Presence of a strong strain in sample B revealed by NIMS1 EPR center. (a) D_{2d} -symmetric distorted structure of NIMS1 center (substitutional P donor). A tetragonal D_{2d} symmetry generates three equivalent orientations along the [100], [010], and [001] axes. The epitaxial growth direction along [111] is also indicated. (b) EPR spectrum of NIMS1 in sample B, when $\mathbf{B} \parallel [110]$. In this \mathbf{B} direction, [001] orientation is distinguishable from other two orientations. In addition to EPR spectrum, the fitting peaks for experimental signals of NIMS1 center and the simulated peaks of NIMS1 center for the ideal population are shown. (c) Population ratios of NIMS centers with three orientations in an ideal uniform population and in sample B. The nonuniform population in sample B indicates the presence of a strong uniaxial strain in P-doped epitaxial layer on Ila-diamond substrate. (d) Schematic view of sample B and its off direction.

D. Strain-induced splitting of nearly degenerate ground states of the P donor in diamond and Li donor in Si

In contrast with the P donor in diamond, the P donor in Si can be easily observed by EPR [6], because the P donor in Si has a singlet (i.e., nondegenerate) a_1 ground state as shown in Fig. 7(a). On the contrary, the interstitial Li donor in Si has a nearly degenerate ground state originating from $t_2 + e$ electronic state [Fig. 7(b)] [26]. These nearly degenerate levels because fast transitions of the electron spins among the energy levels, resulting in strong lifetime broadening. Therefore, the EPR signal of the Li donor is only observable under a strong uniaxial strain that splits the energy levels [Fig. 7(c)]. In the present study, we observed the P donor (the NIMS1 center) only in sample B, which clearly exhibited a strong uniaxial strain. Therefore, by analogy, we assume that the P donor in diamond should have a nearly degenerate ground state [Fig. 7(d)].

Furthermore, the above model is also supported by temperature dependence of the NIMS1 center. As shown in Fig. 8, there is a clear difference in temperature dependence between the experimental data and the case of paramagnetic spins according to Curie's law. The difference is accounted for by the presence of excited states very close to the ground state. It also suggests the presence of the nearly degenerate ground state of the P donor in diamond.

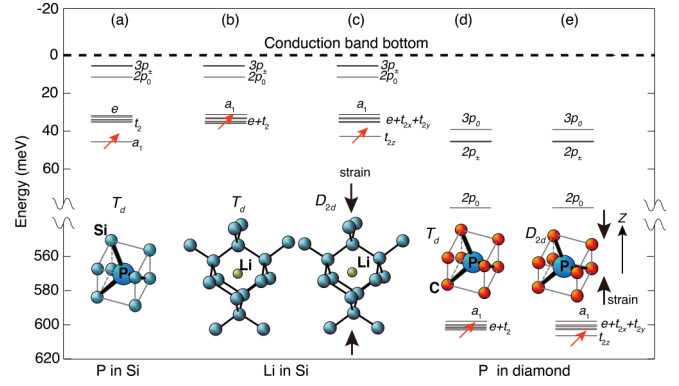


FIG. 7. Schematic illustration of $1s$ ground states and excited states of substitutional P donors in Si and diamond, in addition to those of interstitial Li donors in Si. Electronic states (a_1 , e , and t_2 , etc.) shown in (a), (b), and (c) are taken from Refs. [34]. Excited energy levels ($2p_0$, $2p_{\pm}$, $3p_0$) in (d) and (e) are taken from Ref. [35]. Valley-orbit splitting in $1s$ ground state of P donor are schematically drawn, because they have not yet been determined. Solid arrows represent unpaired electrons occupying each $1s$ ground state. The electronic system of the substitutional P donor in diamond is similar to that of interstitial Li donor in Si.

IV. DISCUSSIONS

A. Why P donor in diamond has no singlet a_1 ground state?

In this section, we explain why the P donor in diamond has a nearly degenerate ground state. Nara *et al.* [30] reported that the Li donor at a tetrahedral-interstitial site surrounded by eight Si atoms [see Fig. 7(b)] has a degenerate ground state of

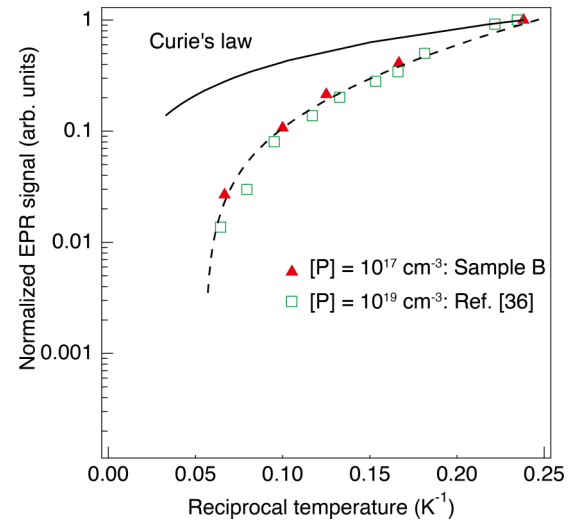


FIG. 8. Temperature dependence of normalized EPR intensity of NIMS1 center. Solid triangles and open squares correspond to EPR measurements on Ila-diamond substrate/P-doped epitaxial film with P doping of $1 \times 10^{17} \text{ cm}^{-3}$ (sample B) and of $1 \times 10^{19} \text{ cm}^{-3}$ (Ref. [36]), respectively. The solid curve indicates normal temperature dependence of EPR intensity according to Curie's law, which was largely separated from experimental results (expressed approximately by a dashed smooth curve). This unusual dependence of the NIMS1 center suggests a close distribution of ground and excited states of substitutional P donor in diamond.

TABLE III. P donor levels, dielectric constants, and wave function parameters of P donor centers in group-IV semiconductors. Fractions of P3s and P3p orbitals, $\eta^2\alpha^2$ and $\eta^2\beta^2$ ($\alpha^2 + \beta^2 = 1$), are calculated from isotropic and anisotropic HF constants A_{iso} and b , via $\eta^2\alpha^2 = |A_{\text{iso}}/A_0|$ and $\eta^2\beta^2 = |b/b_0|$, respectively [38]. We used known isotropic and anisotropic HF constants of $A_0 = 474.79$ mT and $b_0 = 13.088$ mT for ^{31}P [38].

Host element	Donor level (meV)	Dielectric constant	$\eta^2\alpha^2$ (%)	$\eta^2\beta^2$ (%)	η^2 (%)
Si	45 ^a	11.7 ^a	0.88 ^c	0 ^c	0.88 ^c
Ge	12 ^a	15.8 ^a	0.45 ^d	0 ^d	0.45 ^d
diamond	590 ^b	5.8 ^a	0.57 ^{e,f}	11.6 ^{e,f}	12.2 ^{e,f}

^aReference [38].

^bReference [39].

^cReference [6].

^dReference [7].

^eReference [14].

^fThis Work.

$t_2 + e$ because of “the orthogonalization effect” of a 1s core state of the Li donor to a singlet a_1 state. In detail, the interstitial Li donor has a larger amplitude of the wave function at the Li site than that of the Li donor at the substitutional site. In general, the larger amplitude of the wave function on the donor atom causes the stronger orthogonalization effect, which is seen in the following two equations.

$$\psi'_{ki}(\mathbf{r}) = \psi_{ki}(\mathbf{r}) + \sum_{\lambda} (\phi_{\lambda}, \psi_{ki})\phi_{\lambda}(\mathbf{r}) - \sum_{\nu} (\phi_{\nu}, \psi_{ki})\phi_{\nu}(\mathbf{r}), \quad (1)$$

$$\psi'_{ki}(\mathbf{r}) = \psi_{ki}(\mathbf{r}) - \sum_{\nu} (\phi_{\nu}, \psi_{ki})\phi_{\nu}(\mathbf{r}), \quad (2)$$

where $\psi_{ki}(\mathbf{r})$ is a Bloch function for a crystal momentum vector \mathbf{k} and a position \mathbf{r} at the i^{th} of the sixfold valley orbits of a donor in a T_d -symmetric crystal field, and the round brackets indicate the overlap integral of two wave functions. $\psi'_{ki}(\mathbf{r})$ is obtained by orthogonalizing ψ_{ki} with respect to the λ^{th} core state of the host element, $\phi_{\lambda}(\mathbf{r})$, and the ν^{th} core state of the donor atom, $\phi_{\nu}(\mathbf{r})$ [30]. Equations (1) and (2) correspond to the cases of the substitutional donor atom and the tetrahedral-interstitial donor atom, respectively. Note that the Li donor has only the 1s state. Therefore, for Eq. (2) (the interstitial Li donor), only ψ_{ki} of the singlet a_1 state has a nonzero positive coefficient, i.e., the orthogonalization effect:

$$\psi'_{ki}(\mathbf{r}) = \psi_{ki}(\mathbf{r}) - (\phi_{\text{Li}, 1s}, \psi_{k, a_1})\phi_{\text{Li}, 1s}(\mathbf{r}). \quad (3)$$

Therefore, the amplitude of $\psi'_{ki}(\mathbf{r})$ is reduced at the interstitial Li site. This effect lifts up the singlet a_1 electronic level of the a_1 state, resulting in the degenerate $t_2 + e$ ground state [26]. This situation is generally called “inverted group-V-like ground state” [30].

From the ^{31}P HF tensor, we experimentally determine the wave function parameters (3s and 3p orbitals on a P atom) of the NIMS1 center, in addition to those of the P donor centers in Si and Ge, which are summarized in Table III. In the NIMS1 center (P donor in diamond), the spin localization (η^2) on the P donor site is 12.2%, which mostly consists

of 3p orbitals. These features are strikingly in contrast with the cases of Si and Ge. Assuming the same magnitude of the spin localization (12.2%) for the singlet a_1 ground state, we estimate the isotropic HF interaction to be 58 mT. On the contrary, the P donors in Si and Ge show smaller spin localizations due to higher dielectric constants and shallower donor levels than those in diamond (Table III). Due to the larger wave function amplitude of the P donor in diamond, the orthogonalization effect with the respect to the a_1 ground state is stronger in diamond than in Si and Ge. Therefore, it is expected that the P donor in diamond has the a_1 as an excited state [Figs. 7(d) and (e)], while those in Si and Ge have a_1 as a ground state [Fig. 7(a)]. The strong p character of the P donor in diamond is consistent with the t_2 or $t_2 + e$ ground states [Fig. 7(d)] [6].

We also discuss the P1 EPR center [31] that arises from another substitutional group-V impurity in diamond. For the P1 center, first-principles calculations [19,32] predicted that a substitutional nitrogen (N) impurity has a singlet a_1 ground state with a C_{3v} symmetry. Therefore, an electron spin of the P1 center occupies the singlet a_1 state and can be easily observed even at room temperature in various diamond samples [31], which is quite different from the substitutional P donor center (NIMS1 center). This difference between N and P mainly originates from the magnitude of their distortion. The distortion for N is induced by the splitting of bonding and antibonding orbitals between a N lone pair and a C dangling bond along [111] axis [19,32]. It was theoretically predicted that such a distortion results in a 25% elongation of the N-C bond, while six nearest-neighbor C atoms move within only a 3% variation of their three C-C bonds or N-C bonds. As a result, the substitutional N atom has a large energy gain due to the elongation of the N-C bond. For the P1 center, a theoretical calculation estimated the energy gain of the distortion to be 0.63 eV [19], which is much larger than the theoretical energy gain of the Jahn-Teller distortion for the substitutional P atom (4–35 meV) [33].

B. A suggested experimental resolution of previous theoretical discrepancies

In principle, diamond has the same type of conduction band edge (consists of sixfold valleys) as Si and Ge, and their P donors should generate a singlet a_1 state, a doublet e state, and a triplet t_2 state, which are split due to a T_d crystal field of the diamond structure. However, previous theoretical calculations for the ground state of the P donor in diamond are controversial. Jackson *et al.*, Kajihara *et al.*, Sada *et al.*, Wang *et al.*, Seggev *et al.*, and Lombardi *et al.* [18–23] predicted the singlet a_1 ground state, while Orita *et al.*, Butorac *et al.*, and Alferi *et al.* [15–17] predicted the degenerate t_2 ground state. On the basis of our experimental results and the above discussions, we speculate that this controversy may come from the degree of accuracy when calculating the orthogonalization effect with respect to every a_1 , e , and t_2 state of the P atom.

V. SUMMARY

We investigated phosphorus donors in P-doped diamond epitaxial films by means of EPR spectroscopy. In a diamond

thin film on a IIa diamond substrate, we could observe an EPR signal of “NIMS1 center”, which has been assigned to a neutral P donor with a D_{2d} symmetry. On the contrary, we could not observe this center in another free-standing diamond film with the same P concentration ($[P] \sim 1 \times 10^{17} \text{ cm}^{-3}$). This striking contrast can be reasonably explained by proposing that the P donor in diamond has a nearly degenerate ground state of t_2 or $t_2 + e$, in contrast to P donors in group-IV semiconductors like Si and Ge where the a_1 singlet ground state is present. We also observed a strong uniaxial strain only in the former diamond thin film, which was confirmed by Raman microscopy and preferential orientations of the NIMS1 EPR

centers. This strain splits the nearly degenerate ground state of the P donor, resulting in the observation of the NIMS1 centers. Finally, we pointed out that the electronic system of the substitutional P donor in diamond is analogous to that of an interstitial Li donor in Si, where the a_1 singlet ground state is shifted up in energy by the orthogonalization effect.

ACKNOWLEDGMENTS

This work was partially supported by MEXT Q-LEAP (JP-MXS0118067395), JST CREST (JPMJCR1773), and JAEA Project on wisdom integration (30I123).

-
- [1] S. Koizumi, H. Umezawa, J. Pernot, and M. Suzuki, in *Power Electronics Device Applications of Diamond Semiconductors* (Woodhead Publishing, Cambridge, UK, 2018).
- [2] D. D. Awschalom, R. Hanson, J. Wrachtrup, and B. B. Zhou, *Nat. Photonics* **12**, 516 (2018).
- [3] S. Yamanaka, H. Watanabe, S. Masai, D. Takeuchi, H. Okushi, and K. Kjimura, *Jpn. J. Appl. Phys.* **37**, L1129 (1998).
- [4] H. Kato, T. Makino, S. Yamasaki, and H. Okushi, *J. Phys. D* **40**, 6189 (2007).
- [5] E. D. Herbschleb, H. Kato, Y. Maruyama, T. Danjo, T. Makino, S. Yamasaki, I. Ohki, K. Hayashi, H. Morishita, M. Fujiwara, and N. Mizuochoi, *Nat. Commun.* **10**, 3766 (2019).
- [6] A. M. Tyryshkin, S. A. Lyon, A. V. Astashkin, and A. M. Raitsimring, *Phys. Rev. B* **68**, 193207 (2003).
- [7] G. Feher, *Phys. Rev.* **114**, 1219 (1959).
- [8] N. T. Son, J. Isoya, T. Umeda, I. G. Ivanov, A. Henry, T. Ohshima, and E. Janzen, *Appl. Magn. Reson.* **39**, 49 (2010).
- [9] N. D. Samsonenko, V. V. Tokil, and S. V. Gorban, *Sov. Phys. Solid State* **33**, 1409 (1991).
- [10] M. E. Zvanut, W. E. Carlos, J. A. Freitas, Jr., K. D. Jamison, and R. P. Hellmer, *Appl. Phys. Lett.* **65**, 2287 (1994).
- [11] J. Isoya, H. Kanda, M. Akaishi, Y. Morita, and T. Ohshima, *Diam. Relat. Mater.* **6**, 356 (1997).
- [12] N. Casanova, E. Gheeraert, A. Deneuve, C. Uzan-Saguy, and R. Kalish, *Phys. Stat. Solidi A* **181**, 5 (2000).
- [13] T. Graf, M. S. Brandt, C. E. Nebel, M. Stutzmann, and S. Koizumi, *Phys. Stat. Solidi A* **193**, 434 (2002).
- [14] M. Katagiri, J. Isoya, S. Koizumi, and H. Kanda, *Phys. Stat. Solidi A* **203**, 3367 (2006).
- [15] T. Nishimatsu, H. Katayama-Yoshida, and N. Orita, *Jpn. J. Appl. Phys.* **46**, 315 (2007).
- [16] B. Butorac and A. Mainwood, *Phys. Rev. B* **78**, 235204 (2008).
- [17] A. Giovanni, K. Lukas, and M. Anderi, *Phys. Stat. Sol. (RRL)* **12**, 1700409 (2018).
- [18] K. Jackson, M. R. Pederson, and J. G. Harrison, *Phys. Rev. B* **41**, 12641 (1990).
- [19] S. A. Kajihara, A. Antonelli, J. Bernholc, and R. Car, *Phys. Rev. Lett.* **66**, 2010 (1991).
- [20] D. Saada, J. Adler, and R. Kalish, *Appl. Phys. Lett.* **77**, 878 (2000).
- [21] L. G. Wang and A. Zunger, *Phys. Rev. B* **66**, 161202(R) (2002).
- [22] D. Segev and S.-H. Wei, *Phys. Rev. Lett.* **91**, 126406 (2003).
- [23] E. B. Lombardi, A. Mainwood, and K. Osuch, *Phys. Rev. B* **70**, 205201 (2004).
- [24] X. Zhou, G. D. Watkins, K. M. McNamara Rutledge, R. P. Messmer, and S. Chawla, *Phys. Rev. B* **54**, 7881 (1996).
- [25] M. Katagiri, J. Isoya, S. Koizumi, and H. Kanda, *Appl. Phys. Lett.* **85**, 6365 (2004).
- [26] G. D. Watkins and Frank S. Ham, *Phys. Rev. B* **1**, 4071 (1970).
- [27] G. Feher, J. C. Hensel, and E. A. Gere, *Phys. Rev. Lett.* **5**, 309 (1960).
- [28] S. K. Sharma, H. K. Mao, P. M. Bell, and J. Z. Xu, *J. Raman Spectrosc.* **16**, 350 (1985).
- [29] J. W. Ager and M. D. Drory, *Phys. Rev. B* **48**, 2601 (1993).
- [30] H. Nara and A. Morita, *J. Phys. Soc. Jpn.* **23**, 831 (1967).
- [31] C. J. Terblanche and E. C. Reynhardt, *Chem. Phys. Lett.* **322**, 273 (2000).
- [32] G. B. Bachelet, G. A. Baraff, and M. Schlüter, *Phys. Rev. B* **24**, 4736 (1981).
- [33] R. J. Eyre, J. P. Goss, P. R. Briddon, and J. P. Hongon, *J. Phys.: Condens. Matter* **17**, 5831 (2005).
- [34] C. Jagannath, Z. W. Grabowski, and A. K. Ramdas, *Phys. Rev. B* **23**, 2082 (1981).
- [35] M. Willatzen, M. Cardona, and N. E. Christensen, *Phys. Rev. B* **50**, 18054 (1994).
- [36] M. Katagiri, Ph.D. Thesis, University of Tsukuba, 2006.
- [37] J. A. Weil, J. R. Bolton, and J. E. Wertz, in *Electron Paramagnetic Resonance* (Wiley, New York, 1994).
- [38] C. Kittel, in *Introduction to Solid State Physics*, edited by S. Johnson (Wiley, New York, 2004).
- [39] R. Sauer, in *Semiconductors and Semimetals 76*, edited by C. Nebel and J. Ristein (Elsevier, New York, 2003).